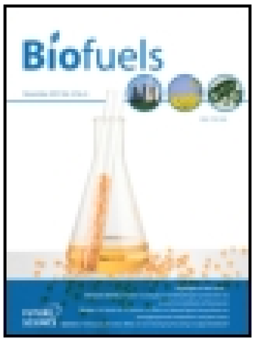

Biofuels

ISSN: 1759-7269 (Print) 1759-7277 (Online) Journal homepage: http://www.tandfonline.com/loi/tbfu20

Effect of bioethanol–diesel blends, exhaust gas recirculation rate and injection timing on performance, emission and combustion characteristics of a common rail diesel engine

Venkatesh T. Lamani, Aditya U. Baliga M, Ajay Kumar Yadav & G. N. Kumar

BIOFUELS, 2017
https://doi.org/10.1080/17597269.2017.1329493

Taylor & Francis
Taylor & Francis Group

Effect of bioethanol–diesel blends, exhaust gas recirculation rate and injection timing on performance, emission and combustion characteristics of a common rail diesel engine

Venkatesh T. Lamani, Aditya U. Baliga M, Ajay Kumar Yadav and G. N. Kumar

Department of Mechanical Engineering, National Institute of Technology Karnataka, Surathkal, Mangalore, 575 025, India

ABSTRACT

This investigation is focused on the effect of exhaust gas recirculation (EGR) and injection timing on the performance, combustion and exhaust emission characteristics of common rail direct injection (CRDI) engine fueled with bioethanol-blended diesel using computational fluid dynamics (CFD) simulation. Simulation is carried out for various EGR rates (0, 10, 20 and 30%), two different injection timings, and two different bioethanol–diesel blends (10 and 20%) at injection pressure. The equivalence ratio is kept constant in all the cases of bioethanol–diesel blends. The results indicate that the mean CO formation and ignition delay increase, whereas mean NO formation and in-cylinder temperature decrease, with increase in the EGR rate. Further, with an increase in percentage of the bioethanol blends, CO and soot formation decrease as compared to neat diesel. A significant increase in in-cylinder pressure (15%) is found at 14° before top dead centre (BTDC) compared to 9° BTDC, which leads to an increase in indicated thermal efficiency of 4% for neat diesel at 30% EGR. In the present study, maximum indicated thermal efficiency is obtained in the case of 10 and 20% bioethanol–diesel blend, and remains constant for all EGR rates considered in the study. Obtained results are validated with the available literature data and indicate good agreement.

ARTICLE HISTORY
Received 9 January 2017
Accepted 27 March 2017

KEYWORDS
CRDI; CFD; exhaust gas recirculation; combustion analysis; biofuel; emission

Nomenclature

D_t	diffusion coefficient
$\dot{\tilde{E}}_{Fu}^{F \to M}$	unmixed fuel source term
$\dot{\tilde{E}}_{O_2}^{A \to M}$	unmixed oxygen source term
ATDC	After top dead centre
BTDC	Before top dead centre
ECFM3Z	extended coherent flame model three zone
EGR	exhaust gas recirculation
EVC	exhaust valve closing
EVO	exhaust valve opening
IMAP	intake manifold air pressure
IMAT	intake manifold air temperature
IVO	inlet valve opening
IVC	inlet valve closing
$\dot{m}_{egr}$	EGR mass flow rate
$\dot{m}_{int}$	total intake mass flow rate
$\dot{m}_a$	mass flow rate of intake air
M_{Fu}	molar mass of fuel
R	universal gas constant
S_c *and* S_{ct}	laminar and turbulent Schmidt numbers
$\bar{S}_{NO}$	mean nitric oxide source term
$\tilde{u}$	density-weighted average velocity
$\bar{\dot{\omega}}_x$	average combustion source term

Greek letters

ζ	transformed coordinate system
$\bar{\rho}^u\|_u$	density of the unburned gases
ε	dissipation rate
ϕ	equivalence ratio
ϕ_s	soot mass fraction
μ	dynamic viscosity
τ_d	ignition delay
$\bar{\rho}$	Reynolds averaged fuel density
$\tilde{Y}_{NO}$	mean mass fraction of NO_x
x_i	Cartesian coordinates
M_{NO}	molar mass
$\frac{dc_{NO\_prompt}}{dt}$	prompt mechanisms
$\frac{dc_{NO\ thermal}}{dt}$	thermal mechanisms
μ_t	turbulent viscosity
$\tilde{Y}_x$	averaged mass fraction of species *x*
M^M	mean molar mass of the gases in the mixed area
M_{Fu}	molar mass of fuel
$M_{air+\ EGR}$	mean molar mass of the unmixed air + EGR gases
$\bar{\rho}$	mean density
$\tilde{Y}_{O_2}^{\infty}$	oxygen mass fraction
τ_m	mixing time
$\tilde{Y}_{TO_2}$	oxygen tracer
$\tilde{Y}_{TFu}$	fuel tracer

CONTACT Ajay Kumar Yadav ajaykyadav@nitk.edu.in

Introduction

Stringent emission regulations, escalation of crude oil price, and depletion of fossil fuel resources have created awareness to find alternate fuels for internal combustion engines. Development of efficient and eco-friendly combustion systems with available alternative fuels has become a challenging task for researchers and automobile manufacturers. Alcohols have been considered as substitute fuels for diesel engines due to their high oxygen content, high stoichiometric air-fuel ratio, high hydrogen-carbon ratio, low sulfur content and high burning rate, which lead to lower emissions [1–6]. Alcohol has a high laminar flame propagation speed, which helps to complete the combustion process early and results in improvement of engine thermal efficiency. Bioethanol has the potential to become the most significant alternative fuel for motor vehicles because it is renewable in nature, and less viscous than diesel fuel [7–11]. Bioethanol is safer for transportation and storage due to its higher auto-ignition temperature than that of diesel [12,13]. Bioethanol can also be produced from waste wood, which has significant potential to reduce CO_2 emission from the life-cycle greenhouse gas [14–18]. An engine operated with ethanol–biodiesel–diesel (EBD) was found to have reduced volatile organic compound at medium load compared to neat diesel operations [19].

Numerous experimental investigations have been carried out to study the influence of bioethanol–diesel blends in diesel engines, and it has been observed that they increase engine performance [20–23].

Engine-out emissions are reported on an engine operated with bioethanol as a fuel, which yields a reduction in smoke [23–30] and, contrarily, an increase in hydrocarbon emissions [31–33]. Beatrice et al. [34] and Labeckas et al. [35] also reported reductions in NO_x and HC emissions for richer combustible mixtures.

Various Computational fluid dynamics (CFD) studies on combustion and emission characteristics of conventional/common rail direct injection (CRDI) engines are carried out for neat diesel [36–39]. Recently, a CFD study on the effects of ethanol addition on biodiesel combustion was carried out for various injection timings, engine loads and blends. For the efficient use of biodiesel/ethanol blend fuels, they suggested that the ethanol blend ratio and advanced fuel injection timing should be carefully selected.

Detailed CFD studies on combustion and emission characteristics of direct injection engines using bioethanol diesel blends are very scant in the open literature. In most of the available literature, the mass of injected fuel per cycle has been kept constant in the case of blending to study the performance of engines, which is not justified because the equivalence ratio may change due to different chemical composition of the fuel [40]. It is well known that the performance of an engine directly depends on equivalence ratio (rich or lean mixture). In the case of ethanol (C_2H_5OH), an extra oxygen atom is already present in the fuel, which can change the air fuel ratio. In this study, we explore the details of variations in engine performance, tailpipe emissions and combustion characteristics for various bioethanol diesel blends, exhaust gas recirculation (EGR) rates, and different injection timings at constant equivalence ratio. The CFD simulation is carried out for a four-stroke CRDI engine to better comprehend the in-cylinder combustion. In-cylinder pressure and temperature, and engine-out emissions of soot, NO and CO are measured. Further in-cylinder pressure traces are considered to determine the heat release rates in terms of ignition delay. Such a study is not currently available in the open literature.

Engine details and fuel properties

Engine details

The CRDI engine used by Mobasheri et al. [38] and Han et al. [39] is considered for CFD simulation in the present work. The details of the engine system and injection system are listed in Table 1.

Fuel properties and combustion strategy

A bioethanol–diesel blend is considered in the present study, with 0 to 20% bioethanol on a mass basis. The neat diesel and ethanol fuel properties are listed in Table 2 [35]. Simulations are carried out for various EGR rates and different injection timings (9° and 14° BTDC). The EGR rate in steady-state operation can be defined as the ratio of EGR mass flow rate ($\dot{m}_{egr}$) to the total intake mass flow rate ($\dot{m}_{\text{int}}$).

$$\dot{m}_{\text{int}} = \dot{m}_a + \dot{m}_{egr} \tag{1}$$

$$EGR = \dot{m}_{egr} \,/\, \dot{m}_{\text{int}} \tag{2}$$

Table 1. Engine specifications [38].

Engine parameters	Values
Bore × stroke	0.13719 m × 0.1651 m
Compression ratio	15.1:1
Connecting rod length	0.26162 m
Displacement	2441 cm^3
IVO/IVC	32° BTDC / 147° BTDC
EVO/EVC	134° ATDC / 29° ATDC
Engine speed	1600 rpm
IMAP	184,000 N/m^2
IMAT	310 K
Injector parameters	Values
Injector type	Common rail
Injection pressure	90 MPa
Number of nozzle holes	6
Nozzle hole diameter	0.00026 m
Injection duration	21.5° CA
Start of injection	9° BTDC
Fuel injected	0.0001622 kg/cycle

Table 2. Properties of ethanol and diesel fuel [35].

Property parameters	Diesel fuel	Ethanol
Molecular formula	$C_{14}H_{24.2}O_{0.8}$	C_2H_5OH
Density at 20°C, kg/m^3	830.5	790
Kinematic viscosity at 40°C, mm^2/s	2.07	1.4
Flash point, open cup, °C	56	13
Boiling point, °C	177–370	78
Auto-ignition temperature, °C	250	365
Cetane number	51.5	8
Oxygen, max wt%	0.4	34.8
Carbon to hydrogen ratio (C/H)	6.9	4
Stoichiometric air–fuel ratio, kg/kg	14.45	9.06
Net heating value, MJ/kg	42.95	26.95
Sulphur mg/kg	2.2	-
Stoichiometric air–fuel ratio, kg/kg	14.2	9.06

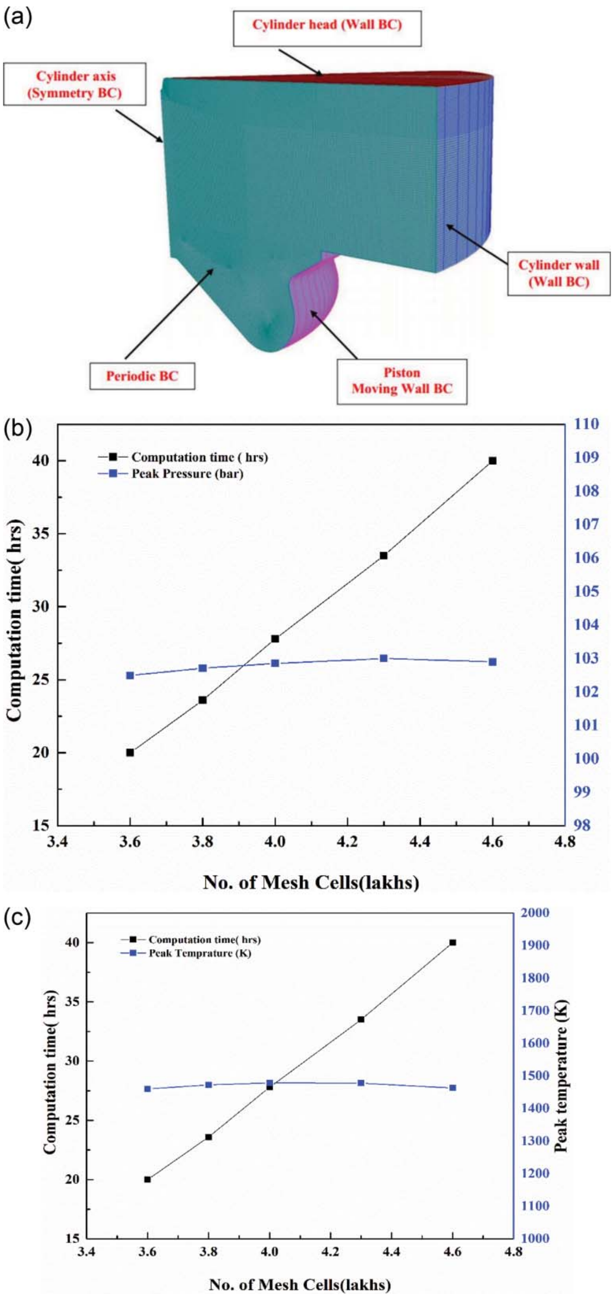

Figure 1. (a) Three-dimensional computational domain at Top dead centre (TDC) position. (b) Grid independence study carried out for peak pressure. (c) Grid independence study carried out for peak temperature.

Table 3. Calculation domain boundaries.

Boundary type	Boundary condition	Values
Piston	Moving mesh	Temperature 550 K
Axis	Periodic inlet/outlet	Periodic
Cylinder head	Wall	Temperature 550 K
Compensation volume	Wall	Thermal/adiabatic boundary
Liner	Wall	Temperature 425 K

Computational model

CFD code and meshing of geometry

The AVL ESE CFD tool is used for engine geometric modelling and computational meshing, as portrayed in Figure 1(a). An injector with six holes is situated centrally on the top of piston; hence, a 60° sector is selected for the computational simulation. In order to reduce the computational time, a high-pressure cycle is considered in the present work. Simulation is started and ended at inlet valve closed and exhaust valve open positions, respectively. A grid independence test was carried out to obtain the optimum grid size, as shown in Figure 1(b) and (c). Simulation is carried out using a 64-GB RAM 16-core work station with parallel processing. The results were checked for peak pressure, peak temperature and computational time for various grid sizes. It was found that the considered parameters are invariant with change in total number of grids at/after 4×10^5. Models employed in the simulation, boundary conditions and range of simulation parameters are listed in Tables 3, 4 and 5, respectively.

Governing equations

The governing equations are listed below.

The transport equation for chemical species is modelled as:

$$\frac{\partial(\bar{\rho}\tilde{Y}_x)}{\partial t} + \frac{\partial(\bar{u}_i\bar{\rho}\tilde{Y}_x)}{\partial x_i} = \frac{\partial}{\partial x_i}\left(\left(\frac{\mu}{S_c} + \frac{\mu}{S_{ct}}\right)\frac{\partial \tilde{Y}_x}{\partial x_i}\right) + \bar{\omega}_x \quad (3)$$

Table 4. Models employed in FIRE software [41].

Turbulence model	k-ζ-f model
Breakup model	Wave
Turbulent dispersion model	Enable
Wall treatment	Hybrid wall treatment
Wall impingement model	Walljet 1
Heat transfer wall model	Standard wall function
Evaporation model	Dukowicz and multi-component model
Combustion model	Coherent flame model (CFM)
Ignition model	Extended coherent flame model 3 zone (ECFM-3Z)
Soot formation and oxidation	Kinetic model
NO_x mechanism	Extended Zeldovich
Chemistry solver	Fire internal chemistry interpreter (CHEMKIN-II)

Table 5. Range of simulation parameters.

Parameters	Range
Blend (% of bioethanol)	0, 10, 20
EGR (%)	0, 10, 20, 30
Injection timings	9° and 14° BTDC
Equivalence ratio	0.47

The fuel transport equations are [42]:

$$\frac{\partial(\bar{\rho}\tilde{Y}^{u}_{Fu})}{\partial t}+\frac{\partial(\bar{\rho}\tilde{u}_i\tilde{Y}^{u}_{Fu})}{\partial x_i}=\frac{\partial}{\partial x_i}\left(\left(\frac{\mu}{S_c}+\frac{\mu_t}{S_{ct}}\right)\frac{\partial\tilde{Y}^{u}_{Fu}}{\partial x_i}\right)+\bar{\rho}\tilde{\bar{S}}^{u}_{Fu}+\bar{\dot{\omega}}^{u}_{Fu}-\bar{\dot{\omega}}^{u\to b}_{Fu} \quad (4)$$

$$\frac{\partial(\bar{\rho}\tilde{Y}^{b}_{Fu})}{\partial t}+\frac{\partial(\bar{\rho}\tilde{u}_i\tilde{Y}^{b}_{Fu})}{\partial x_i}=\frac{\partial}{\partial x_i}\left(\left(\frac{\mu}{S_c}+\frac{\mu_t}{S_{ct}}\right)\frac{\partial\tilde{Y}^{b}_{Fu}}{\partial x_i}\right)+\bar{\rho}\tilde{\bar{S}}^{b}_{Fu}+\bar{\dot{\omega}}^{b}_{Fu}-\bar{\dot{\omega}}^{u\to b}_{Fu} \quad (5)$$

The equations for these unmixed species are:

$$\frac{\partial(\bar{\rho}\tilde{Y}^{F}_{Fu})}{\partial t}+\frac{\partial(\bar{\rho}\tilde{u}_i\tilde{Y}^{F}_{Fu})}{\partial x_i}-\frac{\partial}{\partial x_i}\left(\left(\frac{\mu}{S_c}+\frac{\mu_t}{S_{ct}}\right)\frac{\partial\tilde{Y}^{F}_{Fu}}{\partial x_i}\right)=\bar{\rho}\tilde{\bar{S}}^{F}_{Fu}+\bar{\rho}\tilde{\bar{E}}^{F\to M}_{Fu} \quad (6)$$

$$\frac{\partial(\bar{\rho}\tilde{Y}^{A}_{O_2})}{\partial t}+\frac{\partial(\bar{\rho}\tilde{u}_i\tilde{Y}^{A}_{O_2})}{\partial x_i}-\frac{\partial}{\partial x_i}\left(\left(\frac{\mu}{S_c}+\frac{\mu_t}{S_{ct}}\right)\frac{\partial\tilde{Y}^{A}_{O_2}}{\partial x_i}\right)=\bar{\rho}\tilde{\bar{E}}^{A\to M}_{O_2} \quad (7)$$

The amount of mixing is computed with a characteristic time scale based on the k-epsilon model:

$$\bar{\dot{E}}^{F\to M}_{Fu}=-\frac{1}{\tau_m}\tilde{Y}^{F}_{Fu}\left(1-\tilde{Y}^{F}_{Fu}\frac{\bar{\rho}M^{M}}{\bar{\rho}^{u}|_{u}M_{Fu}}\right) \quad (8)$$

$$\bar{\dot{E}}^{A\to M}_{O_2}=-\frac{1}{\tau_m}\tilde{Y}^{A}_{O_2}\left(1-\frac{\tilde{Y}^{A}_{O_2}}{\tilde{Y}^{\infty}_{O_2}}\frac{\bar{\rho}M^{M}}{\bar{\rho}^{u}|_{u}M_{air+EGR}}\right) \quad (9)$$

τ_m is the mixing time, defined as:

$$\tau_m^{-1}=\beta_m\frac{\varepsilon}{k} \quad (10)$$

whereβ_m is a constant with a default value of 1.

The oxygen mass fraction in unmixed air is computed as follows:

$$\tilde{Y}^{\infty}_{O_2}=\frac{\tilde{Y}_{TO_2}}{1-\tilde{Y}_{TFu}} \quad (11)$$

Pollutant model

The transport equation modelled for nitrogen monoxide [43] is given by:

$$\frac{\partial(\bar{\rho}\tilde{Y}_{NO})}{\partial t}+\frac{\partial(\bar{u}_i\bar{\rho}\tilde{Y}_{NO})}{\partial x_i}=\frac{\partial}{\partial x_i}\left(\bar{\rho}D_t\frac{\partial\tilde{Y}_{NO}}{\partial x_i}\right)+\bar{S}_{NO} \quad (12)$$

The term $\bar{S}_{NO}$ represents NO_x pollutant formation in the equation.

$$\bar{S}_{NO}=M_{NO}\left(\frac{dc_{NO\ thermal}}{dt}+\frac{dc_{NO\ prompt}}{dt}\right) \quad (13)$$

The transport equation modelled for formation mass fraction ϕ_s is given by:

$$\frac{\partial}{\partial t}(\bar{\rho}\tilde{\phi}_s)+\frac{\partial}{\partial x_j}(\bar{\rho}\bar{u}_j\bar{\phi}_s)=\frac{\partial}{\partial x_j}\left(\frac{\mu_{eff}}{\sigma_s}\frac{\partial\bar{\phi}_s}{\partial x_j}\right)+S_{\varphi_s} \quad (14)$$

Soot formation rate is defined as:

$$S_{\varphi_s}=S_n+S_g+S_{o_2} \quad (15)$$

where S_n= soot nucleation, S_g= soot growth and S_{o_2}= soot oxidation.

Validation

In the present study, the engine simulation software AVL-FIRE was coupled with CHEMKIN II with detailed reaction mechanisms. The simulation is validated from the literature [38,39] for conditions listed in Table 1. Results are obtained for in-cylinder pressure and heat release rate versus crank angle, as portrayed in Figure 2. Simulation results show good agreement with published experimental data.

Results and discussion

Effect of various injection timings on in-cylinder pressure

Figure 3(a) depicts the influence of injection timing on in-cylinder pressure. The comparison of in-cylinder pressure for 9° and 14° BTDC injection timings for neat diesel and 10% bioethanol–diesel blends are presented. It is observed that advancing injection timing (14° BTDC) yields higher in-cylinder pressure for neat diesel as well as 10% bioethanol–diesel blend. Even though bioethanol has a lower calorific value, it is interesting to see nearly the same in-cylinder pressure for 10% bioethanol–diesel blend compared to neat diesel, which occurs due to better combustion.

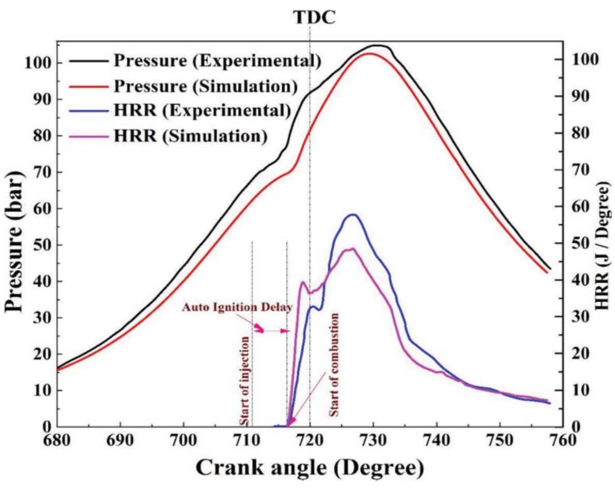

Figure 2. In-cylinder pressure versus crank angle experimental and simulation.

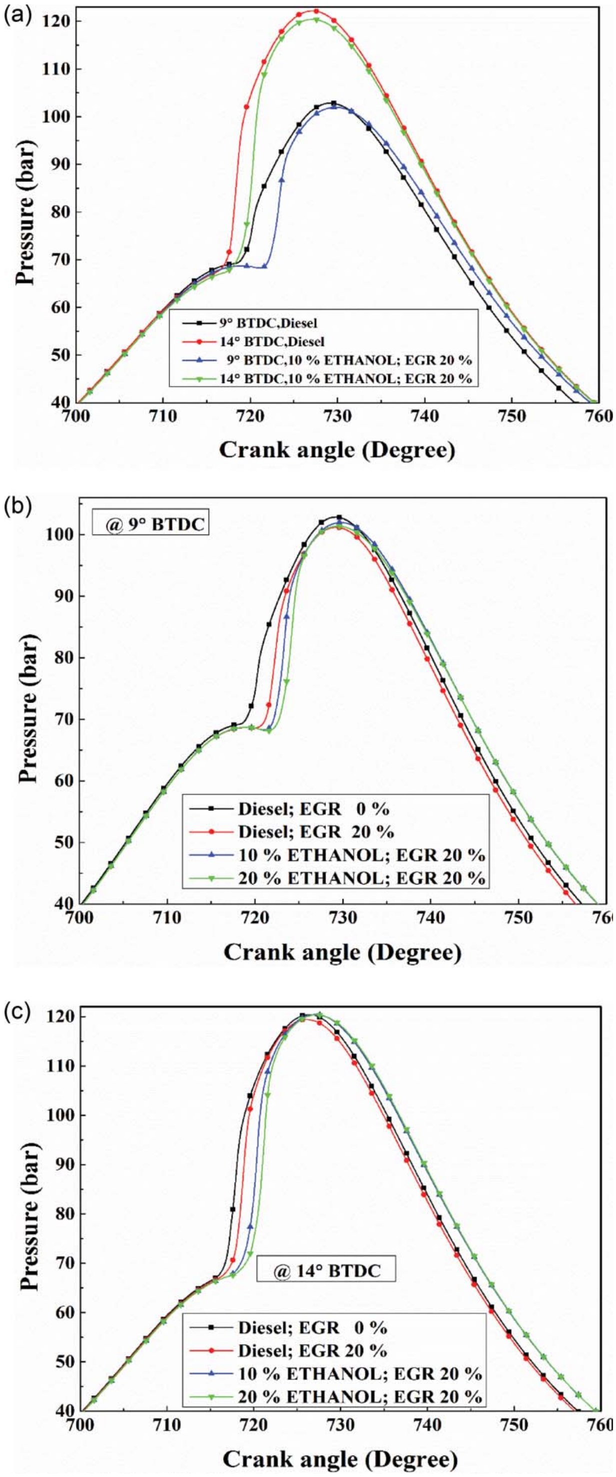

Figure 3. (a) Comparison of in-cylinder pressures for diesel and 10% bioethanol–diesel blends without EGR. Effect of various bioethanol–diesel blends with 20% EGR rate on in-cylinder pressure at (b) 9° BTDC (c) 14° BTDC injection timing.

Effect of various bioethanol–diesel blends on in-cylinder pressure

The diesel engine combustion is partially premixed and partially diffusive. Figure 3(b) and (c) shows the in-cylinder pressure development during the combustion of various fuel blends with 20% EGR rate for injection timing 9° and 14° BTDC, respectively. The in-cylinder peak pressure in the case of bioethanol–diesel blends is less than that of the neat diesel for 9° BTDC, which occurs due to the lower calorific value of bioethanol compared to diesel. On the other hand, in-cylinder pressure for 14° BTDC is approximately the same; due to the low viscosity of bioethanol, better spray and combustion characteristics were achieved.

Effect of different EGR on in-cylinder pressure

Figure 4(a) and (b) shows the in-cylinder pressure development during the combustion of a 10% bioethanol–diesel blend with different EGR for injection timings of 9° and 14° BTDC, respectively. EGR had various effects on fuel charge such as a dilution effect, ignition delay effect, chemical effect and thermal effects, leading to a marginal (1%) decrease in peak pressure in both cases (9° and 14° BTDC).

Effect of various bioethanol–diesel blends on in-cylinder temperature

Figure 5 (a) and (b) shows the in-cylinder temperature during the combustion of various fuel blends with 20% EGR rate for injection timings of 9° and 14° BTDC,

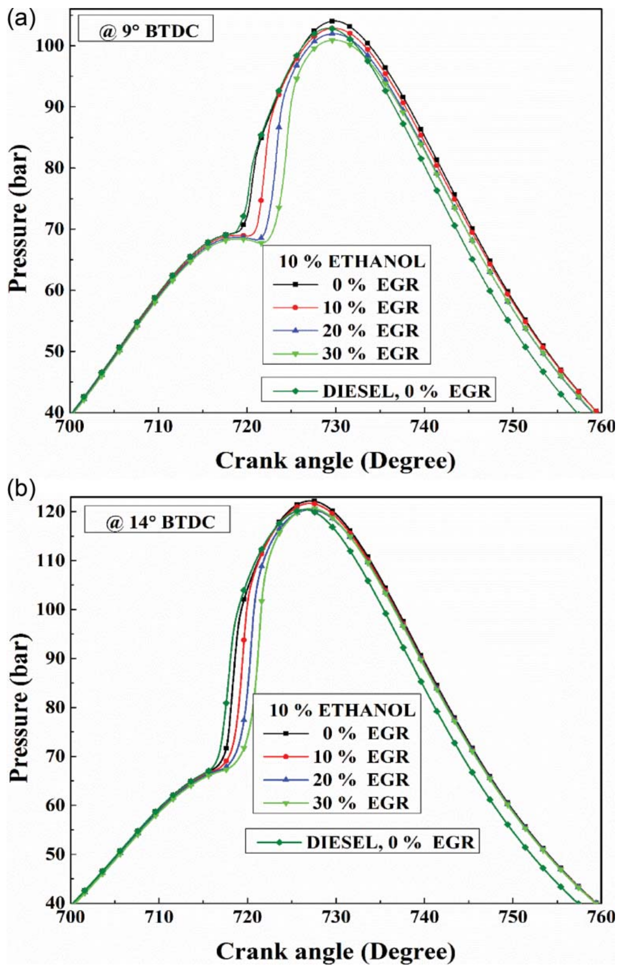

Figure 4. Effect of various EGR rates with 10% bioethanol–diesel blend on in-cylinder pressure for injection timings (a) 9° BTDC and (b) 14° BTDC.

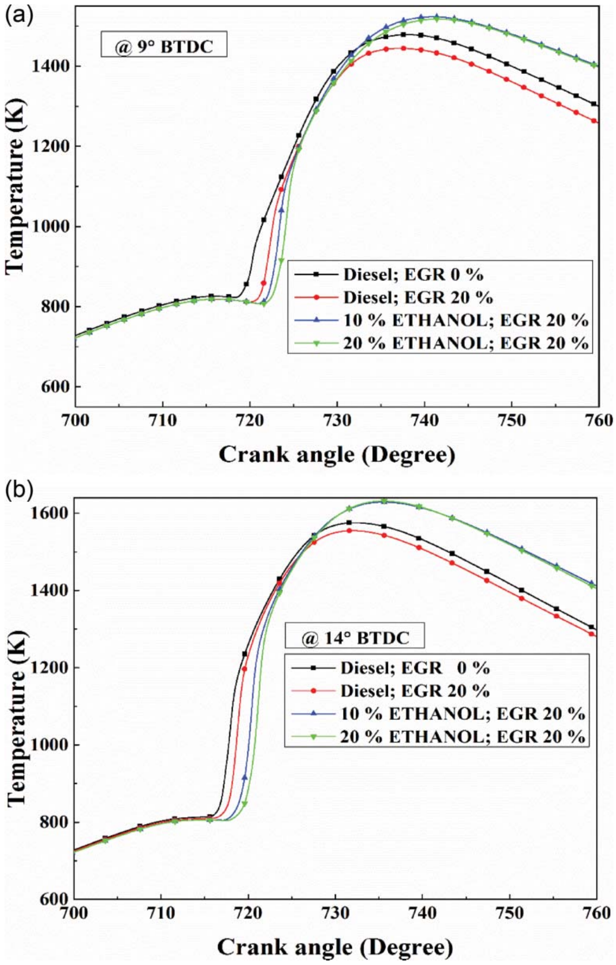

Figure 5. Effect of various bioethanol–diesel blends with 20% EGR rate on in-cylinder temperature for injection timings (a) 9° BTDC and (b) 14° BTDC.

respectively. It has been observed that in-cylinder temperatures for bioethanol–diesel blends (10 and 20% bioethanol) are less than that of neat diesel in pre-flame combustion, and more in post-flame combustion.

Effect of different EGR on in-cylinder temperature

Figure 6(a) and (b) shows the in-cylinder temperature during the combustion of a 10% bioethanol–diesel blend with different EGR for injection timings of 9° and 14° BTDC, respectively. EGR reduces the percentage of oxygen in the combustion chamber, which results in a decrease in temperature due to a dilution effect, as well as thermal and chemical effects. The endothermic dissociation of EGR components (H_2O) contributes to reduce the combustion temperatures [44]. Further, the specific heat capacity of the fuel mixture increases due to a higher CO_2 percentage, which reduces the adiabatic flame temperature. A higher in-cylinder peak temperature difference (90 K) is observed in the case of 14° BTDC compared to 9° BTDC injection timing.

Figure 6(c) shows the development of in-cylinder average temperature for various crank angles. Three-dimensional temperature contours are shown for 10% bioethanol–diesel blend with different EGR rates, at injection timing of 14° BTDC. Temperature contours are plotted for various crank angles (706°, 720° (TDC), 730°, 740°). These contour plots exhibit a clear picture of the combustion process occurring inside the cylinder. The in-cylinder temperature contours offer the opportunity to achieve a deeper insight into in-cylinder temperature distribution in diesel and ethanol combustion.

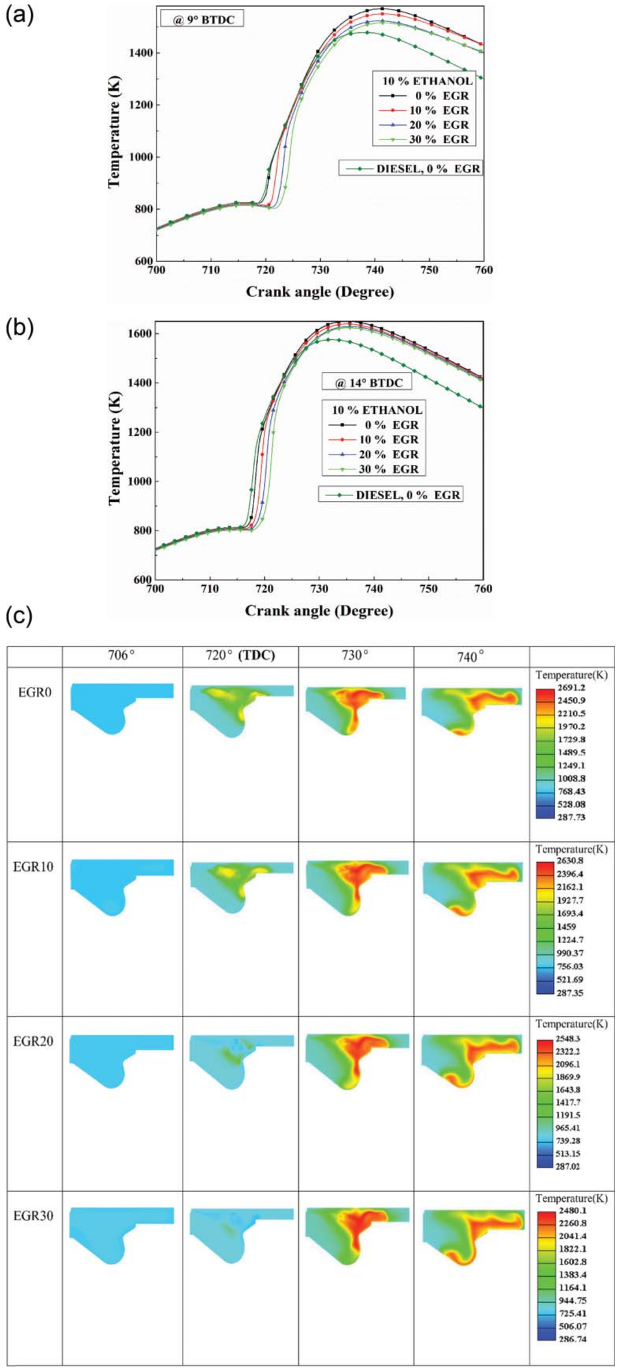

Figure 6. (a) Effect of various EGR rates with 10% bioethanol–diesel blend on in-cylinder temperature for injection timings at 9° BTDC. (b) Effect of various EGR rates with 10% bioethanol–diesel blend on in-cylinder temperature for injection timings at 14° BTDC. (c) Temperature contours of 10% bioethanol–diesel blend at 14° BTDC injection timing and various EGR rates: 0, 10, 20 and 30%.

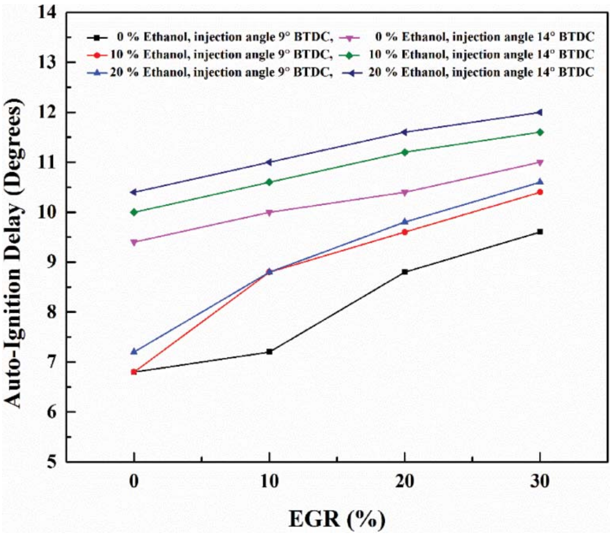

Figure 7. Autoignition delay versus EGR rate for different fuel blends and injection timings.

Effect of EGR on auto-ignition delay

Auto ignition delay is calculated as the difference between the fuel injection timing and the time at which the in-cylinder heat release rate curve appears. Figure (7) shows the influence of EGR on ignition delay for various fuel blends and injection timings. Cetane number plays a decisive role in the start of combustion. Bioethanol has a lower cetane number, which increases the ignition delay as the percentage of bioethanol in the fuel increases. Higher latent heat of vaporization of the fuel (bioethanol) causes lower in-cylinder temperature and hence escalates the ignition delay. The results show that a higher EGR rate increases the ignition delay due to a low oxygen concentration. For all cases of advanced injection timing, the ignition delay is more as expected.

Effect of various bioethanol–diesel blends on NO formation

Figure 8(a) and (b) shows the formation of in-cylinder NO during the combustion of various fuel blends with 20% EGR rate for injection timings of 9° and 14° BTDC, respectively. For 9° BTDC and a 20% EGR rate, NO formation for 10 and 20% bioethanol–diesel blends is increased by 33 and 16%, respectively, compared to neat diesel (20% EGR). Results for neat diesel without EGR are also provided for comparison. For injection timing of 14° BTDC and a 20% EGR rate, NO formation for 10 and 20% bioethanol–diesel blends is decreased by 27 and 31%, respectively, compared to neat diesel (20% EGR). For all cases of advanced injection timing, NO formation increases due to an increase in in-cylinder temperature.

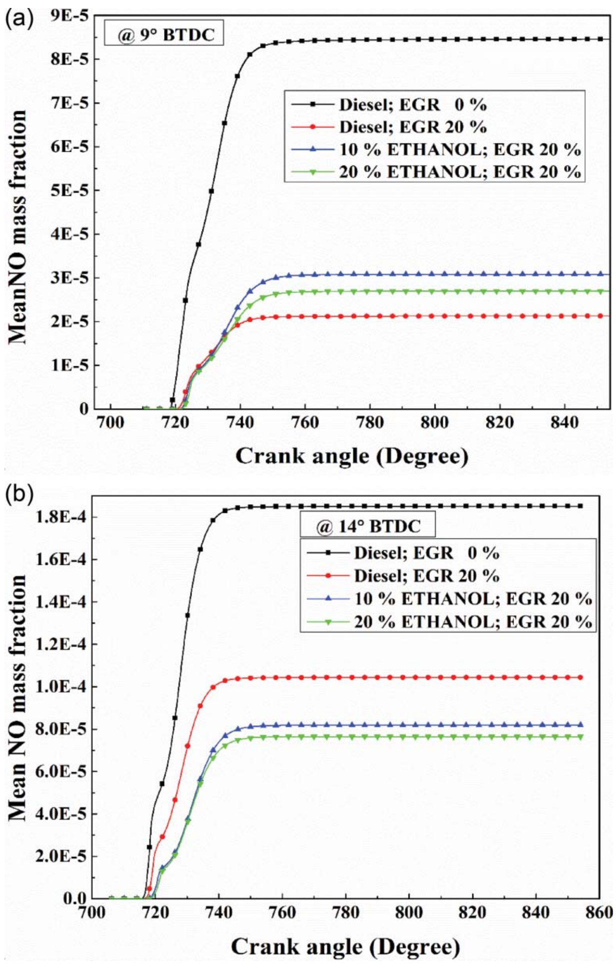

Figure 8. Effect of various bioethanol–diesel blends with 20% EGR rate on NO formation for injection timings (a) 9° BTDC and (b) 14° BTDC.

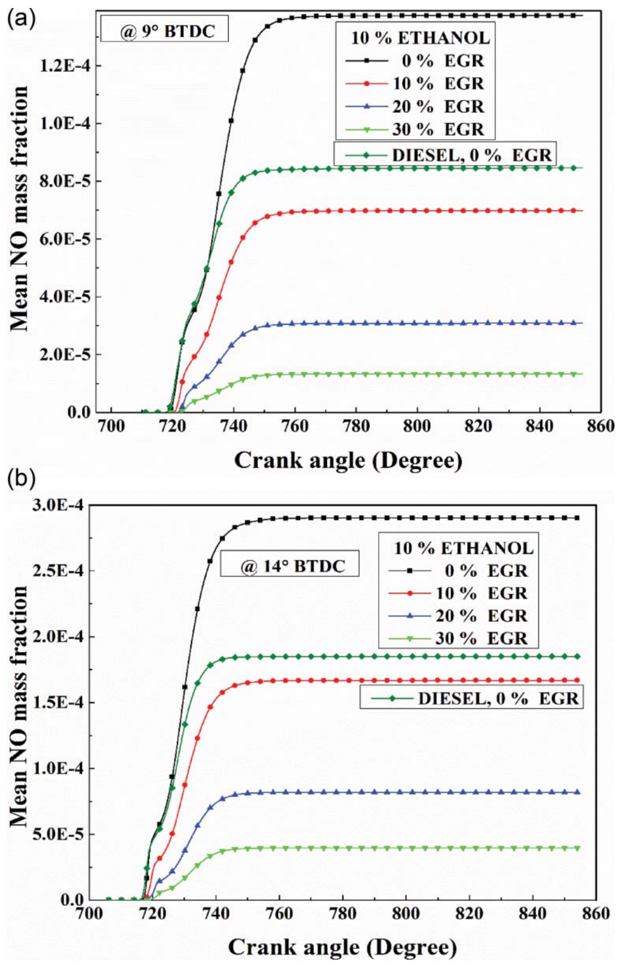

Figure 9. Effect of various EGR rates with 10% bioethanol–diesel blend on NO formation for injection timings (a) 9° BTDC and (b) 14° BTDC.

Effect of EGR rate on in-cylinder NO mass fraction

Figure 9 (a) and (b) shows the formation of the in-cylinder NO mass fraction during the combustion of a 10% bioethanol–diesel blend with different EGR rates for injection timings of 9°and 14° BTDC, respectively. As the overall in-cylinder temperature decreases drastically with an increase in EGR rate, the mean NO formation is reduced.

For injection timing of 9° BTDC and 10% bioethanol–diesel blend, NO formation is decreased by 46, 76 and 90% for 10, 20 and 30% EGR rates, respectively, compared to 0% EGR. A similar trend was observed for 14° BTDC.

Effect of various bioethanol–diesel blends on in-cylinder mean CO mass fraction

Figure 10(a) and (b) shows the formation of the in-cylinder CO mass fraction during the combustion of various fuel blends with a 20% EGR rate for injection timings of 9°and 14° BTDC, respectively. It was found that at constant EGR, CO formation is higher in the case of neat diesel compared to that of blends. For injection timing of 9° BTDC and a 20% EGR rate, CO formation for 10 and 20% bioethanol–diesel blends is decreased by 34 and 70% compared to the neat diesel at 0 and 20% EGR rates, respectively. A similar trend is followed in the case of 14° BTDC. Results for neat diesel without EGR are also provided for comparison. The oxygen content of bioethanol is higher than that of diesel, which causes the conversion of CO in fuel-rich regions into CO_2.The same trend was also observed by Ajay et al. [45].

Effect of different EGR on in-cylinder mean CO mass fraction

Figure 11(a) and (b) shows the formation of the in-cylinder CO mass fraction during the combustion of a 10% bioethanol–diesel blend with different EGR for injection timings of 9°and 14° BTDC, respectively. It is interesting to note that for both injection timings (9°and 14° BTDC), CO formation is lower for the bioethanol diesel blend with EGR (10, 20 and 30%) compared to without-EGR neat diesel operations.

During fossil fuel combustion, CO formation is an intermediate step. In a later phase, with the help of OH

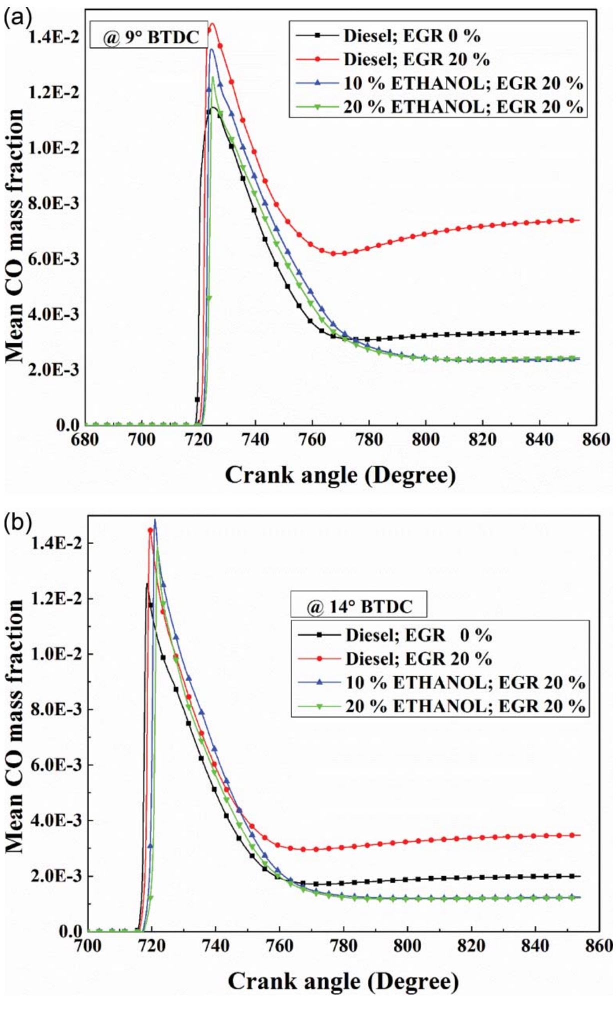

Figure 10. Effect of various bioethanol–diesel blends with 20% EGR rate on CO formation for injection timings (a) 9° BTDC and (b) 14° BTDC.

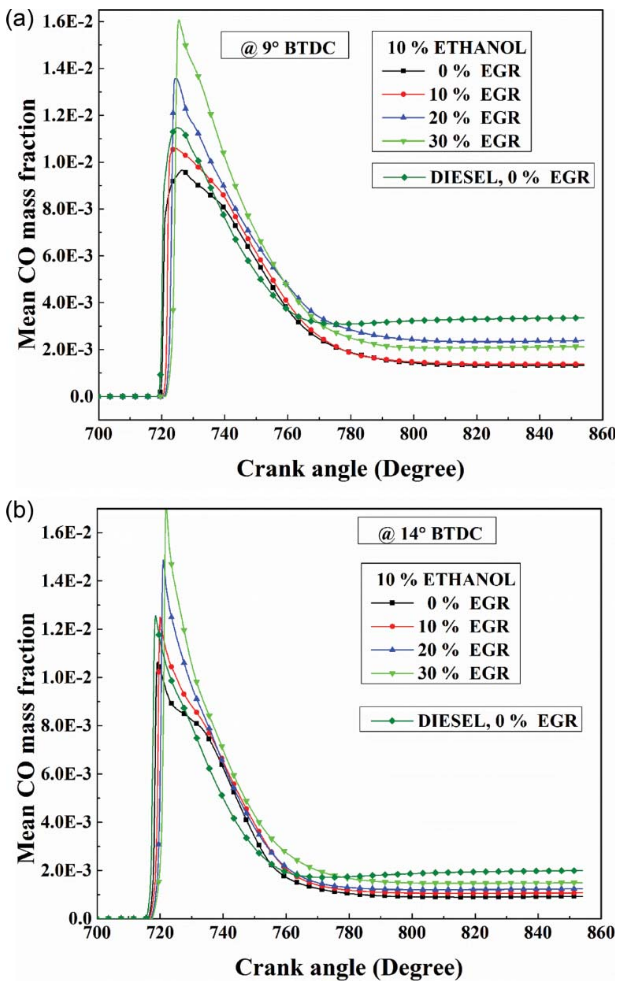

Figure 11. Effect of various EGR rates with 10% bioethanol–diesel blend on CO formation for injection timings (a) 9° BTDC and (b) 14° BTDC.

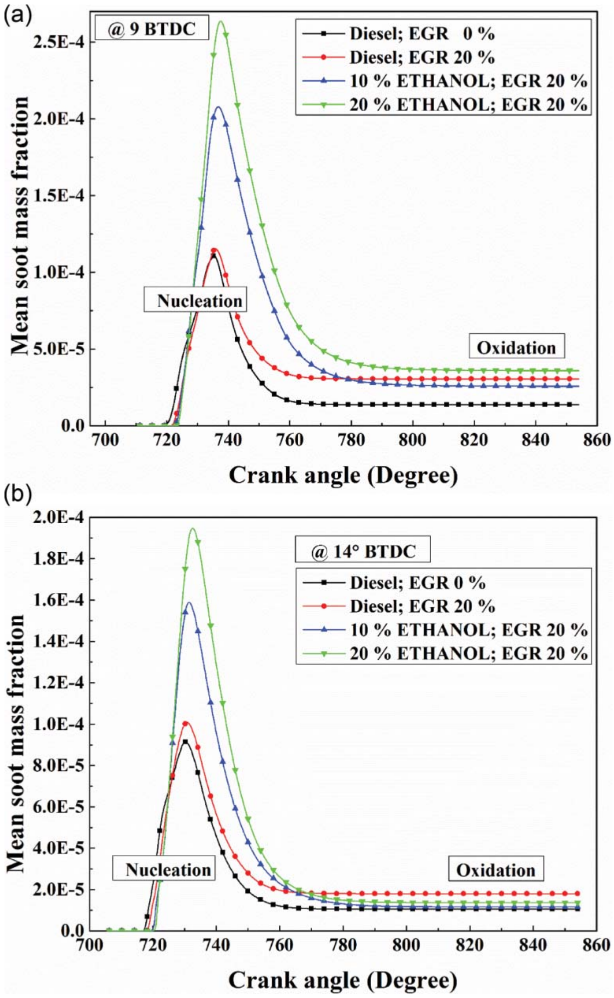

Figure 12. Effect of various bioethanol–diesel blends with 20% EGR rate on soot formation for injection timings (a) 9° BTDC and (b) 14° BTDC.

radicals, in the presence of oxygen inside the cylinder, oxidation occurs and CO_2 is formed at temperatures above 1200 K [46]. If less oxygen is available locally the oxidation of CO stops due to improper mixing of fuel and air. With a higher EGR rate, charge is diluted and more CO is formed.

Effect of various bioethanol–diesel blends on in-cylinder mean soot mass fraction

Figure 12(a) and (b) shows the formation of the in-cylinder mean soot mass fraction during the combustion of various fuel blends with a 20% EGR rate for injection timings of 9° and 14° BTDC, respectively. For an injection timing of 9° BTDC and 20% EGR, the reduction in soot formation for a bioethanol–diesel blend of 10% is 15%, and an increase in soot was observed for the 20% blend of 4%, compared to neat diesel with EGR 20%.

Soot emission can be reduced remarkably with bioethanol addition to diesel fuel at an injection timing of 14° BTDC. The reduction in soot formation was found to be 40 and 25% for injection timing of 14° BTDC and 20% EGR, for 10 and 20% bioethanol blends, respectively, compared to the neat diesel.

The improvement of soot emission can be explained by the enrichment of oxygen owing to bioethanol, resulting in a high local air-fuel ratio which promotes the oxidation of soot nuclei in fuel combustion. Bioethanol reduces the initial radicals for the formation of aromatic rings, which are considered the soot precursors, mainly through reducing the amount of carbon that is available to form precursor species. Wu et al. [47] found that bioethanol-blended fuel decreases the soot due to the formation of OH radicals, as shown in Equation (16):

$$\begin{aligned} C_2H_5OH &\rightarrow C_2H_4 + H_2O \\ H_2O + H &\rightarrow OH + H_2 \end{aligned} \tag{16}$$

Effect of EGR rate on in-cylinder mean soot mass fraction

Figure 13(a) and (b) shows the formation of the in-cylinder soot mass fraction during the combustion of a

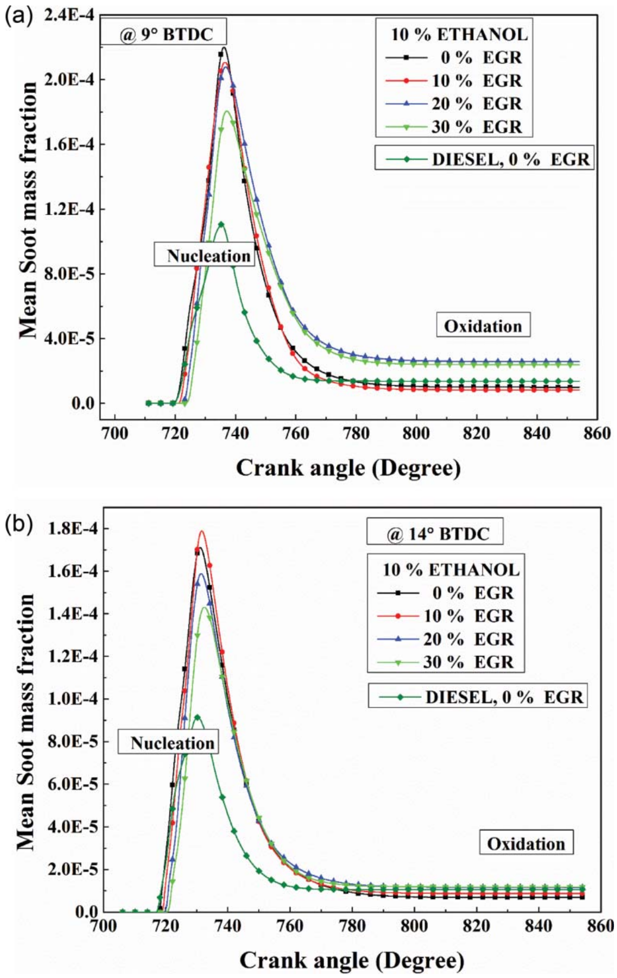

Figure 13. Effect of various EGR rates with 10% bioethanol–diesel blend on soot formation for injection timings (a) 9° BTDC and (b) 14° BTDC.

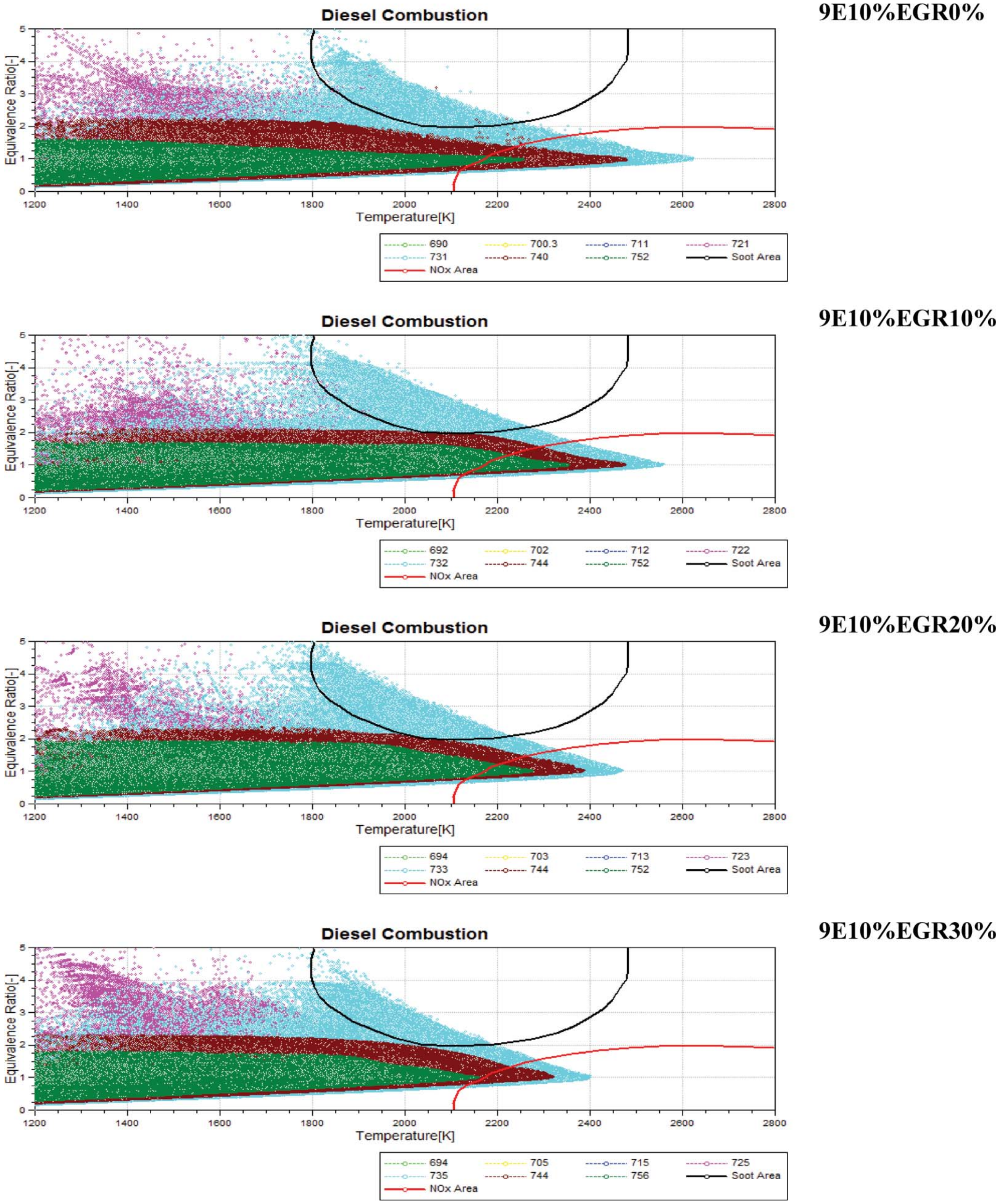

Figure 14. Effect of various EGR rates (0, 10, 20 and 30%) at injection timing 9° BTDC and with 10% bioethanol–diesel blend on equivalence ratio-temperature.

10% ethanol–diesel blend with different EGR for injection timings of 9° and 14° BTDC, respectively. The increase of soot with an increase in the EGR rate, due to a dilution effect, is a well-established fact. But it is interesting to see the lower soot formation for a 10% bioethanol–diesel blend with 0 and 10% EGR, compared to neat diesel without EGR.

For an injection timing of 9° BTDC and 10% ethanol–diesel blend, soot formation for EGR rates of 0 and 10% is decreased by approximately 21% compared to neat diesel without EGR, whereas soot formation is increased by approximately 40% for 20 and 30% EGR rates.

For 14° BTDC and a 10% bioethanol–diesel blend, soot formation for EGR rates of 0 and 10% is decreased by 25 and 20% and increased by 15 and 16%, respectively. With an advance in injection timing, soot decreases.

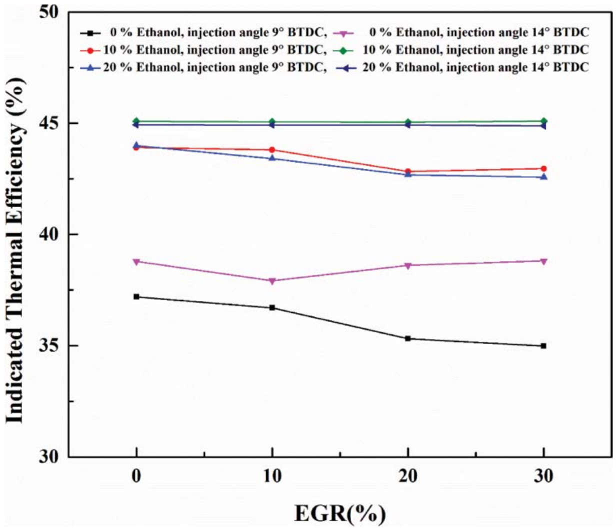

Figure 15. Indicated thermal efficiency versus EGR rate for different bioethanol–diesel blends and injection timings.

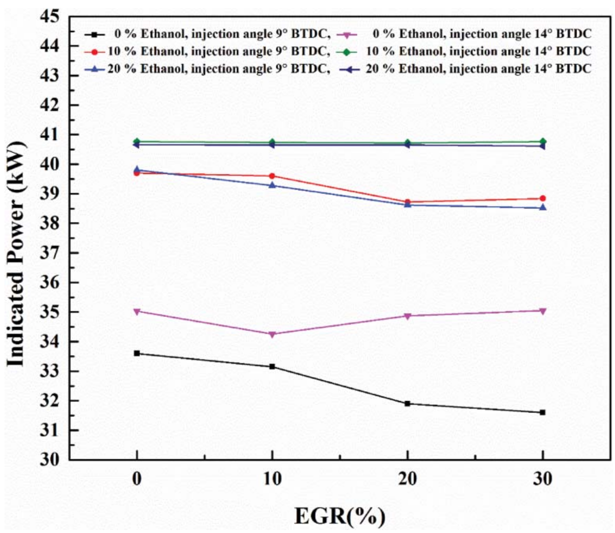

Figure 16. Indicated power versus EGR rate for different bioethanol–diesel blends and injection timings.

Effect of EGR rate and injection timing on equivalence ratio versus temperature

Figure 14 shows the equivalence ratio versus temperature for a 10% bioethanol/diesel blend with various EGR rates. Injection timing and bioethanol blend are held constant at 9° BTDC and 10%, respectively, whereas EGR rate is varied from 0 to 30% (9E10%EGR0%, 9E10%EGR10%, 9E10%EGR20% and 9E10%EGR30%). In this study, 720° Crank angle (CA) is considered TDC and all the engine parameters are employed. It was observed that the majority of NO formation starts at 731°, 732°, 733° and 735 °CA for 0, 10, 20 and 30% EGR rates, respectively, and the maximum peak horizontal NO penetration was witnessed at the 0% EGR rate. As the EGR rate increases NO formation decreases, and less NO is found with the 30% EGR rate. On the other hand, soot continuously increased with an increase in EGR rate, and more soot was observed for 20 and 30% EGR rates.

Effect of various injection timings and EGR rate on engine performance

Figures 15 and 16 show the variation of indicated thermal efficiencies and indicated power with EGR rates for different injection timings (9° and 14° BTDC) and bioethanol–diesel blends, respectively. Higher indicated thermal efficiency (ITE, 4%) as well as higher indicated power (4%) are obtained in all the cases of 14° BTDC injection timing compared to 9° BTDC, which occurs due to high in-cylinder pressure, as explained above. The maximum ITE is observed in the case of 14° BTDC injection timing and 10% bioethanol–diesel blend, and found to be constant for all EGR rates. A similar trend is observed for 9° BTDC injection timing.

Conclusions

A CFD analysis of a four-stroke CRDI engine with bioethanol–diesel blends at various EGR rates and injection timings was carried out. The following conclusions are based on the obtained simulation results:

- For more advanced injection (14° BTDC), higher in-cylinder pressure (15%) is observed in all studied cases, which leads to an increase in the indicated thermal efficiency by approximately 4%, compared to 9° BTDC.
- In the present study, the maximum indicated thermal efficiency is obtained in the case of a 10% bioethanol–diesel blend, for all EGR rates.
- For injection timing of 9° BTDC and a 20% EGR rate, NO formation for 10 and 20% bioethanol–diesel blends is increased by 33 and 16%, respectively, compared to neat diesel (20% EGR).
- For injection timing of 9° BTDC and a 10% bioethanol–diesel blend, NO formation is decreased by 46, 76 and 90% for 10, 20 and 30% EGR rates, respectively, compared to 0% EGR.
- Mean CO formation during combustion is less in the case of bioethanol blends compared to neat diesel.
- For injection timing of 14° BTDC and a 20% EGR, the reduction in soot formation for bioethanol–diesel blends of 10 and 20% is 40 and 25%, respectively, compared to neat diesel with EGR 20%.
- A higher latent heat of vaporization and lower cetane number of bioethanol escalate the ignition delay.

Acknowledgements

The authors would like to acknowledge AVL-AST, Graz, Austria, for the granted use of AVL-FIRE under the University Partnership Program.

Disclosure statement

No potential conflict of interest was reported by the authors.

References

[1] Kisenyi J, Savage C, Simmonds A. The impact of oxygenates on exhaust emissions of six European cars. SAE Technical Paper 940929. Warrendale, PA: Society of Automotive engineers(SAE); 1994.

[2] Di Y, Cheung CS, Huang Z. Experimental study on particulate emission of a diesel engine fueled with blended ethanol-dodecanol-diesel. J Aerosol Sci. 2009;40:101–12.

[3] Imdadul HK, Masjuki HH, Kalam MA, et al. Higher alcohol-biodiesel-diesel blends: An approach for improving the performance, emission, and combustion of a light-duty diesel engine. Energ Convers Manage. 2016;111:174–185.

[4] Adelman H. Alcohols in diesel engine. SAE paper no.790956. Warrendale, PA: Society of Automotive engineers (SAE); 1979.

[5] An H, Yang WM, Li J. Effects of ethanol addition on biodiesel combustion: A modeling study. Appl Energ. 2015;143:176–188.

[5] Zhu L, Cheung CS, Zhang WG, et al. Emission's characteristics of a diesel engine operating on biodiesel and biodiesel blended with ethanol and methanol. Sci Total Environ. 2010;408:914–921.

[6] Britto RF, Martins CA. Experimental analysis of a diesel engine operating in Diesel–Ethanol Dual-Fuel mode. Fuel. 2014;134:140–150.

[7] Singh AP, Agarwal AK. Combustion characteristics of diesel HCCI engine: An experimental investigation using external mixture formation technique. Appl Energ. 2009;99:116–125.

[8] Maurya RK, Agarwal AK. Experimental study of combustion and emission characteristics of ethanol fuelled port injected homogeneous charge Compression ignition (HCCI) combustion engine. Appl Energ. 2011;88:1169–80. DOI:10.1016/j.apenergy.2010.09.015

[9] Can O, Celikten I, Usta N. Effects of ethanol addition on performance and emissions of a turbocharged indirect injection diesel engine running at different injection pressures. Energy Convers Manage. 2004;45:2429–40.

[10] Szwaja S, Naber JD. Combustion of n-butanol in a spark-ignition IC engine. Fuel. 2010;89:1573–82.

[11] Bayraktar H. An experimental study on the performance parameters of an experimental CI engine fueled with diesel-methanol-dodecanol blends. Fuel. 2008;87:158–64.

[12] Furey RL, Perry KL. Composition and reactivity of fuel vapor emissions from gasoline-oxygenate blends. SAE Technical Paper No. 912429.Warrendale, PA: Society of Automotive engineers (SAE); 1991.

[13] Naegeli DW, Lacey PI, Alger MJ, et al. Surface corrosion in ethanol fuel pumps. SAE Technical Paper 971648; Warrendale, PA: Society of Automotive engineers (SAE); 1997.

[14] Boretti A. Advantages of converting diesel engines to run as dual fuel ethanol-diesel. Appl Thermal Eng. 2012;47:1–9.

[15] Beer T, Grant T. Life-cycle analysis of emissions from fuel ethanol and blends in Australian heavy and light vehicles. J Clean Prod. 2007;15:833–837.

[16] Beer T, Grant T, Williams D, et al. Fuel-cycle greenhouse gas emissions from alternative fuels in Australian heavy vehicles. Atmos Environ. 2002;36:753–763.

[17] Jeuland N, Montagne X, Gautrot X. Potentiality of ethanol as a fuel for dedicated engine [C]. In: IFP international conference, which fuels for low CO2 engines? Paris, 2004;07–19.

[18] Owen K, Coley T. Automotive fuels reference book. Warrendale, PA: Society of Automotive engineers (SAE); 1995.

[19] Dinesha P, Nayak V, Shankar KS, et al. Studies on the environmental emission and performance of a single cylinder CI engine with enhanced intake air oxygen combustion. Biofuels. 2014;5(6):713–721.

[20] Maurya RK, Agarwal AK. Experimental investigation on the effect of intake air temperature and air–fuel ratio on cycle-to-cycle variations of HCCI combustion and performance parameters [J]. Appl Energ. 2011;88:1153–1163.

[21] Lei J, Shen L, Bi Y, et al. A novel emulsifier for ethanol-diesel blends and its effect on performance and emissions of diesel engine. Fuel. 2012;93:305–311.

[22] Zhu L, Cheung CS, Zhang WG, et al. Combustion, performance and emission characteristics of a DI diesel engine fueled with ethanol-biodiesel blends. Fuel. 2011;90:1743–1750.

[23] Rakopoulos DC, Rakopoulos CD, Kakaras EC, et al. Effects of ethanol–diesel fuel blends on the performance and exhaust emissions of heavy duty DI diesel engine. Energ Convers Manage. 2008;49:3155–3162.

[24] Ahmed I. Oxygenated diesel: emissions and performance characteristics of ethanol-diesel blends in CI engines [J]. SAE Technical Paper No. 2001-01-247.Warrendale, PA: Society of Automotive engineers (SAE); 2001.

[25] Xing-cai L, Jian-Guang Y, Wu-Gao Z, et al. Effect of cetane number improver on heat release rate and emissions of high speed diesel engine fueled with ethanol–diesel blend fuel. Fuel. 2004;83:2013–2020.

[26] He BQ, Shuai SJ, Wang JX, et al. The effect of ethanol blended diesel fuels on emissions from a diesel engine. Atmos Environ. 2003;37:4965–71.

[27] Zhang RD, He H, Shi XY, et al. Preparation and emission characteristics of ethanol–diesel fuel blends. J Environ Sci. 2004;16:793–796.

[28] Nicholas C, Surawski ZD, Ristovski RJ, et al. Gaseous and particle emissions from an ethanol fumigated compression ignition engine. Energy Convers Manage. 2012;54:145–51.

[29] Dinesha P, Mohanan P. Evaluation of combustion, performance and emissions of a diesel engine fueled with bio-fuel produced from cashew nut shell liquid. Biofuels. 2015;6:101–106.

[30] Kima H, Choi B. Effect of ethanol-diesel blend fuels on emission and particle size distribution in a common-rail direct injection diesel engine with warm-up catalytic converter. Renew Energ. 2008;33:2222–2228.

[31] Fang Q, Fang J, Zhuang J, et al. Effects of ethanol-diesel-biodiesel blends on combustion and emissions in premixed low temperature combustion. Appl Therm Eng. 2013;54:541–548.

[32] Yilmaz N, Vigil FM, Burl Donaldson A, et al. Investigation of CI engine emissions in biodiesel-ethanol-diesel blends as a function of ethanol concentration. Fuel. 2014;115:790–793.

[33] Yilmaz N, Vigil FM. Potential use of a blend of diesel, biodiesel, alcohols and vegetable oil in compression ignition engines. Fuel. 2014;124:168–172.

[34] Beatrice C, Napolitano P, Guido C. Injection parameter optimization by DoE of a light-duty diesel engine fed by

Bio-ethanol/RME/diesel blend. Appl Energ. 2014;113:373–384.

[35] Labeckas G, Slavinskas S, Mazeika M. The effect of ethanol–diesel–biodiesel blends on combustion, performance and emissions of a direct injection diesel engine. Energ Convers Manage. 2014;79:698–720.

[36] Jayashankara B, Ganesan V. Effect of fuel injection timing and intake pressure on the performance of a DI diesel engine – A parametric study using CFD. Energy Convers Manage. 2010;51:1835–1848.

[37] Pang KM, Ng HK, Gan S. Investigation of fuel injection pattern on soot formation and oxidation processes in a light-duty diesel engine using integrated CFD-reduced chemistry. Fuel. 2012;96:404–418.

[38] Mobasheri R, Peng Z, Mirsalim SM. Analysis the effect of advanced injection strategies on engine performance and pollutant emissions in a heavy duty DI-diesel engine by CFD modeling. Int J Heat Fluid Fl. 2012;33:59–69.

[39] Han Z, Uludogan A, Hampson GJ, et al. Mechanism of soot and NOx emission reduction using multiple-injection in a diesel engine. SAE Technical Paper (No. 960633); Warrendale, PA: Society of Automotive engineers (SAE); 1996

[40] Soni DK, Gupta R. Emission control using methanol, ethanol and butanol in diesel engine: A comparison through CFD simulation. IOSR Journal of Mechanical and Civil Engineering. 2015;12:17–23.

[41] FIRE v2011 Manuals. Graz, Austria: AVL LIST GmbH; 2011.

[42] Colin O, Benkenida A. The 3-zones extended coherent flame model (ECFM3Z) for computing premixed/diffusion combustion. Oil Gas Sci Technol. 2004;59:593–609.

[43] Kuo KK. Principles of combustion. India: Wiley; 1986.

[44] Qi D, Leick M, Liu Y, et al. Effect of EGR and injection timing on combustion and emission characteristics of split injection strategy DI-diesel engine fuelled with biodiesel. Fuel. 2011;90:1884–1891.

[45] Ajay EA, Singh B, Bhattacharya TK. Experimental study of some performance parameters of a constant speed stationary diesel engine using ethanol–diesel blends as fuel. Biomass Bioenerg. 1999;17:357–365.

[46] Petranovic Z, Vujanovic M, Duic N. Towards a more sustainable transport sector by numerically simulating fuel spray and pollutant formation in diesel engines. J Clean Prod. 2014;88:272–279.

[47] Wu J, Song Ki H, Litzinger T, et al. Reduction of PAH and soot in premixed ethylene–air flames by addition of ethanol. Combust Flame. 2006;144:675–687.